American Mineralogist, Volume 75, pages 367–380, 1990

Calculated mineral equilibria in the pelite system, KFMASH (K_2O-FeO-MgO-Al_2O_3-SiO_2-H_2O)

Roger Powell
Department of Geology, University of Melbourne, Parkville, Victoria 3052, Australia
Tim Holland
Department of Earth Sciences, University of Cambridge, Downing Street, Cambridge CB2 3EQ, United Kingdom

Abstract

Using the internally consistent thermodynamic data set of Holland and Powell (1990), we have calculated invariant and univariant equilibria in the system KFMASH (K_2O-FeO-MgO-Al_2O_3-SiO_2-H_2O) and the subsystems KFASH and KMASH, involving combinations of staurolite, chloritoid, chlorite, biotite, cordierite, garnet, andalusite, sillimanite, and kyanite with muscovite, quartz, and H_2O in excess, in the pressure-temperature range of 0–18 kbar and 460–720 °C. We not only find the pressure-temperature positions of these equilibria, but also determine the compositions of the minerals involved, in terms of $MgFe_{-1}$ and $MgSiAl_{-2}$ substitutions. Agreement with the petrologically consistent grid of Harte and Hudson (1979) is remarkably good, except that in our KFMASH system grid, without Fe^{3+} there is no stability field for the assemblages chloritoid + biotite or andalusite + biotite. However, taking into account uncertainties in the position of the reactions in the grid and considering small additions of Fe^{3+} into biotite and chloritoid at reasonable concentrations, these assemblages become stable in the grid. We test whether an internally consistent data set such as ours can reasonably predict phase relations as complex as those of natural pelites. Although agreement with petrological observation is surprisingly good, further experimental work is required, particularly for reactions involving cordierite and staurolite, before further improvements to such calculated grids can be made.

Introduction

Attempts to model pelitic reactions in terms of a phase diagram in the simple system K_2O-FeO-MgO-Al_2O_3-SiO_2-H_2O (KFMASH) have increased in sophistication since the earlier work of Albee (1965) and Hess (1969), which were based upon observations of natural assemblages coupled with a knowledge of compositions of coexisting phases. A second generation of grids, exemplified by those of Harte and Hudson (1979, Fig. 2), Labotka (1981), and Holdaway et al. (1982) and improving on Harte (1975), were derived through the combination of petrological observation with experimental results on reactions in the subsystems KMASH and KFASH, providing constraints on the *P-T* position of KFMASH univariant reactions. The grid of Harte and Hudson was able to account for most of the important pelitic facies sequences found as well as the then-available experimental data; nevertheless several assumptions were made in parts of the grid where constraining data were lacking.

A third generation of KFMASH grids, which have been calculated from the thermodynamic data, is now becoming available; these have the merit of allowing the whole grid to be calculated once the thermodynamic data have been chosen. The first of these, Spear and Cheney (1989, Fig. 2), involved a combination of measured and estimated volumes, entropies, and heat capacities. In their grid, they employed a minimum of experimental and petrological constraints on the *P-T* position of reactions in KFASH and KMASH and Fe-Mg partitioning data for the minerals. The grid was designed to be thermodynamically and petrologically consistent.

We take a different approach in this paper in that we attempt for the first time to calculate the KFMASH grid entirely from thermodynamic data using our new, expanded data set (Holland and Powell, 1990), without recourse to any arguments based on field relations or compositions of phase assemblages in the pelite system. Thus we wished to test the ability of our thermodynamic data to predict complex phase relations in the pelite system, particularly to see whether it might be possible to predict not only the *P-T* locations of the univariant reactions, but also the compositions of coexisting phases as a function of pressure and temperature. The approach used is described in greater detail in two of our other petrogenetic grid papers (Guiraud et al., 1989; Will et al., 1990). The grid was assembled from the calculated positions of all the univariant equilibria in KFASH, KMASH, and KFMASH via the application of Schreinemakers's rules. The process is simplified by the requirement that a *stable* KFMASH univariant line must emanate from each *stable* KFASH and KMASH invariant point.

0003–004X/90/0304–0367$02.00

KFMASH GRID

The results of our calculations on the in- and univariant equilibria are summarized as pressure-temperature (P-T) projections for the KMASH and KFASH subsystems in Figure 1, and the full system KFMASH in Figure 2, with a representative collection of results presented in Table 1. The pressure and temperature range was chosen to include most of the greenschist and amphibolite facies; also we chose to consider only the AFM projection system (Thompson, 1957, 1979), and hence our grid refers to excess H_2O, quartz, and phengitic white mica (henceforth called muscovite). The grid shows reactions that involve the following minerals: st = staurolite, g = garnet, bi = biotite, chl = chlorite, ky = kyanite, and = andalusite, sill = sillimanite, cd = cordierite, and ctd = chloritoid, in addition to the excess phases mu = muscovite, q = quartz, and H_2O. In the text, "a" is used for aluminosilicate, one of andalusite, sillimanite, or kyanite. In our P-T window, we have chosen not to include the muscovite + quartz breakdown reactions at low pressure and high temperature, or one talc-bearing KFMASH equilibrium that affects only magnesian-rich compositions, or, indeed, silicate melt equilibria at higher temperatures. All of the thermodyamic data used may be found in the tables of Holland and Powell (1990).

In generating the P-T projection, we took account of two types of solid solution in the minerals: Fe-Mg exchange ($FeMg_{-1}$) and Tschermak's substitution ($(Mg,Fe)SiAl_{-2}$). Ideal mixing was assumed on the sites in the minerals on which the substitutions take place; this assumption was used in the generation of the thermodynamic data themselves, and we thus maintain the internal consistency that helps to minimize the effects of our assumption. Also, importantly, we believe that by making the most reasonable choices of activity model we can reduce the magnitude of the errors involved with the assumption of ideality. For example, we prefer to restrict mixing of Al to only two out of the six octahedral sites in chlorites, such that the entire range of possible Al substitution extends from zero to two, as seems to be the case in nature. The activity models used are in Appendix 1.

In order to illustrate the calculation process and the information generated (by the computer program THERMOCALC—Powell and Holland, 1988), we focus on the classic Barrovian staurolite isograd reaction, which in AFM is chl + g = st + bi, which links the [ctd,and] and [ctd,cd] invariant points (Fig. 2a). To locate the temperature of this reaction at specified pressure we need to solve nine independent equilibrium relations in order to find the nine variables specifying this univariant assemblage: x_{st}, x_g, x_{chl}, y_{chl}, x_{bi}, y_{bi}, x_{mu}, y_{mu} as well as T. For phase i, x_i represents Fe/(Fe + Mg), and y_i represents the extent of Tschermak's substitution (see App. 1 for details). The nine equilibrium relations are nonlinear equations, which we solve by Newton's method with a step-length algorithm, and the resulting mineral compositions and temperature, at specified pressures, are in Table 1a and illustrated in the P-x projection (Fig. 3). Considering the whole length of this reaction, including the stable and metastable parts, we can see how much variation in $FeMg_{-1}$ as well as $(Mg,Fe)SiAl_{-2}$ can occur along the length of such a reaction. The Fe/(Fe + Mg) ratio in chlorite changes from 0.80 to 0.16 as pressure increases from 2 to 14 kbar, and similar changes are also found for staurolite, biotite, and muscovite. This reaction emanates from a metastable KMASH invariant point at about 20 kbar and terminates at a metastable KFASH invariant point at less than 1 kbar. In terms of Tschermak's substitution, biotite varies from eastonitic (y_{bi} = 0.5) at 2 kbar to only slightly less aluminous compositions (y_{bi} = 0.33) at 14 kbar, whereas muscovites become quite phengitic at 14 kbar, with y_{mu} dropping from 0.91 to 0.73.

Some features of Figures 1 and 2 are worthy of note:

1. In Figure 1, the [cd,bi,chl] invariant point occurs in the kyanite and in the andalusite field, as a consequence of the marked deflection of the reactions across the aluminosilicate polymorph reactions. The stability of the two invariant points have a controlling effect on the grids with, for example, the staurolite field in KFASH, and thus also KFMASH, being closed to high and low pressure.

2. The KFASH invariant points, [st,bi,and] and [st,bi,chl], lie very close to the KFMASH invariant [bi,st], at slightly lower temperatures (along the KFASH reaction, ctd = cd). Corresponding KFMASH reactions extend down temperature from [bi,st] and terminate at these invariant points. As can be seen in Table 1b, the phases in the reactions in and around [bi,st] (and [bi,cd] and [bi,ctd]) are all very Fe-rich.

3. The strong curvature of the KFASH reactions, chl + ctd = g and chl = bi + g, is caused by the relatively rapid change of Tschermak's substitutions in the minerals along the reactions, particularly the increasingly aluminous nature of chlorite with decreasing pressure and/or increasing temperature. The data compiled by Laird (1988, p. 413, Fig. 6) for natural pelitic rocks show precisely this same trend. In our example, y_{chl} in the first of these reactions increases from 0.52 at 11 kbar to 0.72 at 3 kbar, and for the second reaction, 0.34 to 0.68. Noting that in AFM, 2Al/(Fe + 2Al) = y_{chl}/3, chlorite crosses the garnet composition at y_{chl} = 0.75; the resulting g = chl singularity is metastable at 1.5 kbar. The absence of a chloritoid + biotite field of stability in Figure 2 is a result of the nonintersection of these KFASH reactions; the key KFMASH univariant reaction, g + chl = ctd + bi, would emanate to lower temperature from the resulting invariant point.

4. The absence of an andalusite + biotite field of stability in Figure 2B is precluded by the stability of st + cd and, particularly, g + cd. The g + cd field (Fig. 2B) extends to low temperatures, terminating at the KFASH invariant point [st,bi,and] (Fig. 1), but the coexisting mineral compositions are very Fe-rich below about 600 °C (Table 2a). Note however that the uncertainty on the position of sill + bi = cd + g, a reaction that controls the

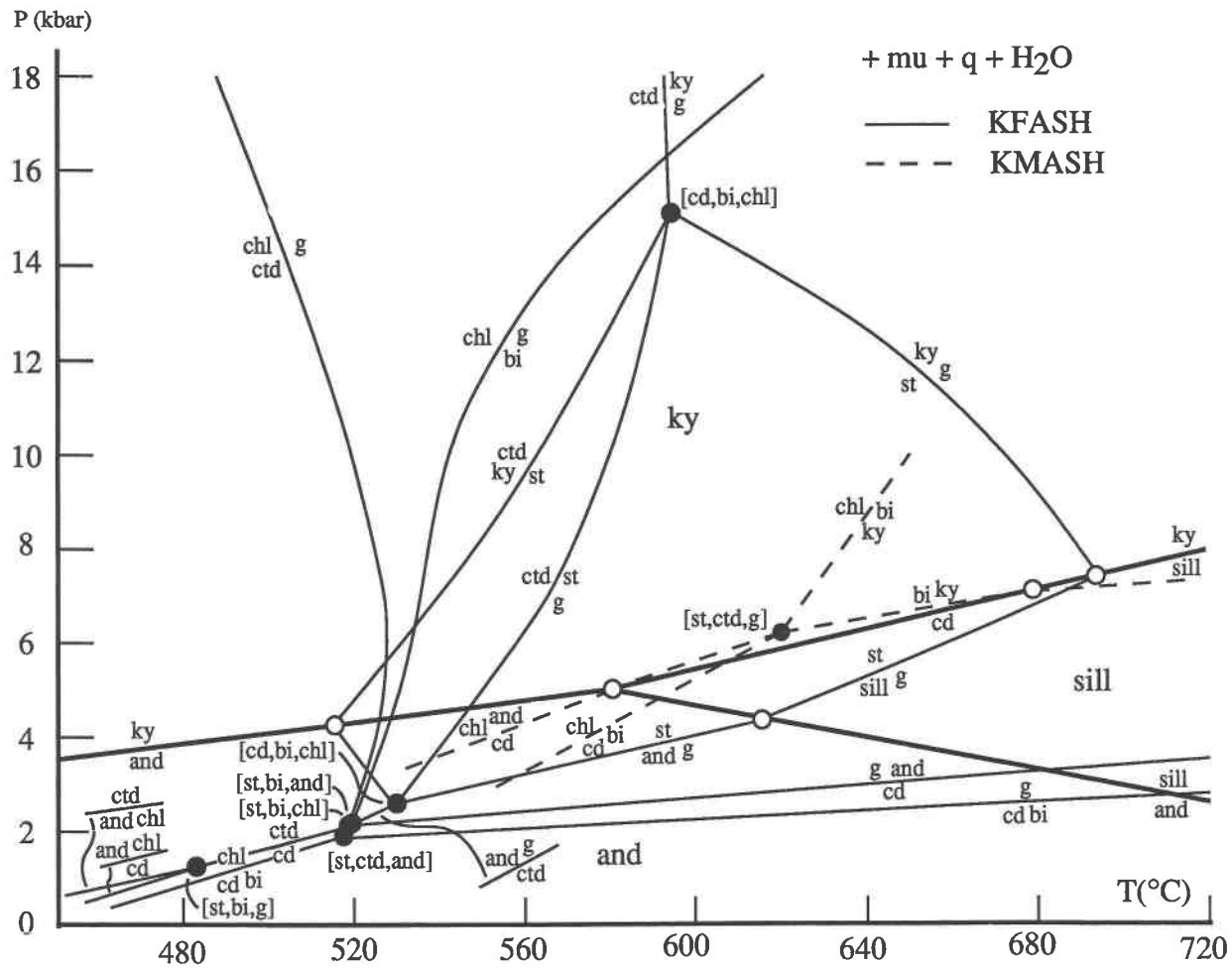

Fig. 1. Pressure-temperature projection for KFASH (solid lines) and KMASH (dashed lines). Note that a KFMASH univariant line (in Fig. 2) emanates from each of the invariant points in this diagram.

stability of bi + and in KFMASH, is of the order of ±2 kbar (at 2σ); as and + bi = cd + g has a steeper dP/dT than sill + bi = cd + g, if cd + g is destabilized, a large bi + and field is generated.

5. The position of the aluminosilicate triple point is the one calculated from the data in the internally consistent data set. Note that experimental results on the position of the andalusite = sillimanite reaction were *not* included in the generation of the data set because of the inconsistencies among various studies (Holland and Powell, 1985; Holland and Powell, 1990). The calculated position of andalusite = sillimanite is a consequence of the positions of all the other equilibria involving these aluminosilicates used in the data-set generation. Although some may prefer a lower temperature for the triple point, note that the calculated temperature of the triple point is 580 ± 50 °C (at 2σ).

P-x projections are a good way of summarizing mineral composition relationships along invariant lines and at invariant points (e.g., Thompson, 1976; Thompson et al., 1977; Powell, 1978). Figure 3 shows a *P-x* projection of the phase relations in the kyanite field; the two invariant points are represented by horizontal lines linking the compositions of coexisting phases, and the individual univariant equilibria are shown by groups of lines giving the compositions of the phases involved in each. The information in this diagram must be combined with the *P-T* projection (Fig. 2) so that the temperature associated with the particular univariant equilibrium can be determined. An important feature is that all the equilibria, with the exception of st + ctd = g + ky and st + chl = g + ky, are characterized by increasingly magnesian mineral compositions as pressure increases. The conditions of formation and mineral compositions presented in Figure 2 and Figure 3 compare well with those deduced from natural assemblages [e.g., the Gassetts schist data (Thompson et al., 1977; their Fig. 8)].

A more approachable way of viewing the dependence of phase relations on the changing mineral compositions along univariant lines is via isobaric *T-x* pseudosections and *P-T* pseudosections (e.g., Hensen, 1971; Thompson, 1976; Powell, 1978; Labotka, 1981). The *T-x* pseudosec-

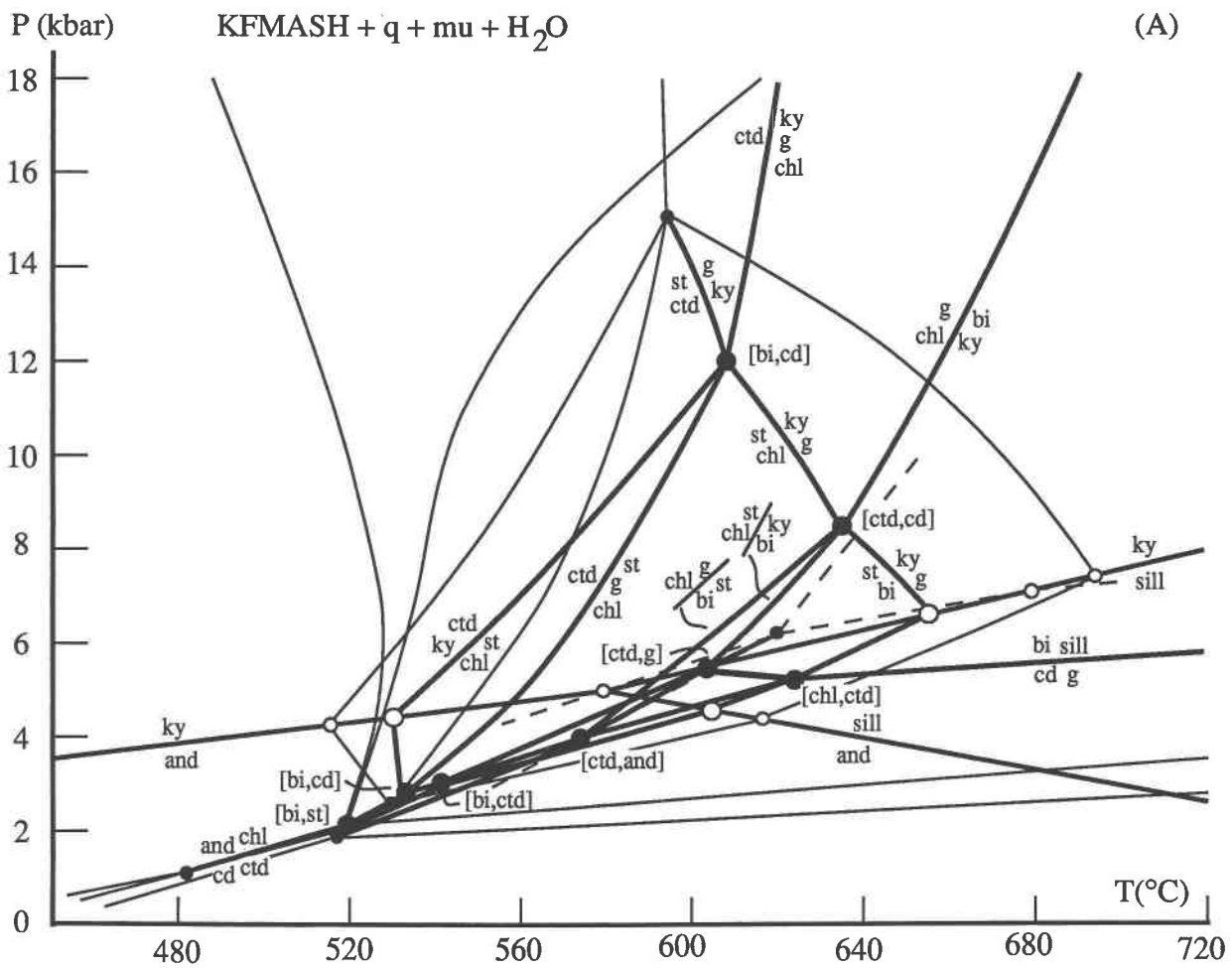

Fig. 2. Pressure-temperature projection for KFMASH. Note that KFMASH univariant lines either terminate at KFASH or KMASH invariant points (Fig. 1) or at KFMASH invariant points. (A) The projection for the full range of pressure and temperature.

tion in Figure 4 was calculated for 6-kbar pressure for a complete range of Fe/(Fe + Mg) at constant Al/(Mg + Fe), i.e., for a horizontal line on the AFM projection below that of the g + chl tie-line. Figure 4, calculated entirely from thermodynamic data extracted from experiments in simple chemical systems, compares quite well with natural pelite associations (e.g., Fig. 10 of Labotka, 1981, drawn for the slightly more aluminous compositions corresponding to the garnet-chlorite join). For compositions with intermediate Fe/(Fe + Mg) ratios, the classic Barrovian sequence is displayed as temperature increases. The convergence of the sill + cd + bi and g + sill + bi fields at 730 °C leads to the stabilization of g + cd by the univariant reaction sill + bi = g + cd. Of note are the particularly narrow fields for chl + ky + bi and chl + cd + bi, implying that the incoming of cordierite at low and moderate pressures will make a good isograd, at least in rocks close to KFMASH.

The *P-T* pseudosection in Figure 5 was drawn for a composition with Fe/(Fe + Mg) = 0.7 at an Al/(Fe + Mg) just below that of g + chl in AFM. Given the way the Fe/(Fe + Mg) ratios of the coexisting minerals change along the univariant lines, it is important to construct such pseudosections to see which, and how much of each, equilibria are "seen" by a particular rock. For example, note that the greatest majority of the equilibria in Figure 2b in the andalusite field are not "seen" by this bulk composition, or in fact by any "normal" pelite, because the mineral compositions in these equilibria are very Fe rich. Moreover, most of these equilibria lie within each other's uncertainty limits, and therefore the locations of the reactions and thus the topology are uncertain. For more magnesian compositions most of the divariant fields in Figure 5 are located at higher pressure and temperature.

Comparison with the Harte and Hudson grid

Comparison of our calculated grid with that of Harte and Hudson (1979, Fig. 2) amounts to checking it for geologic consistency, given the success of this grid at ac-

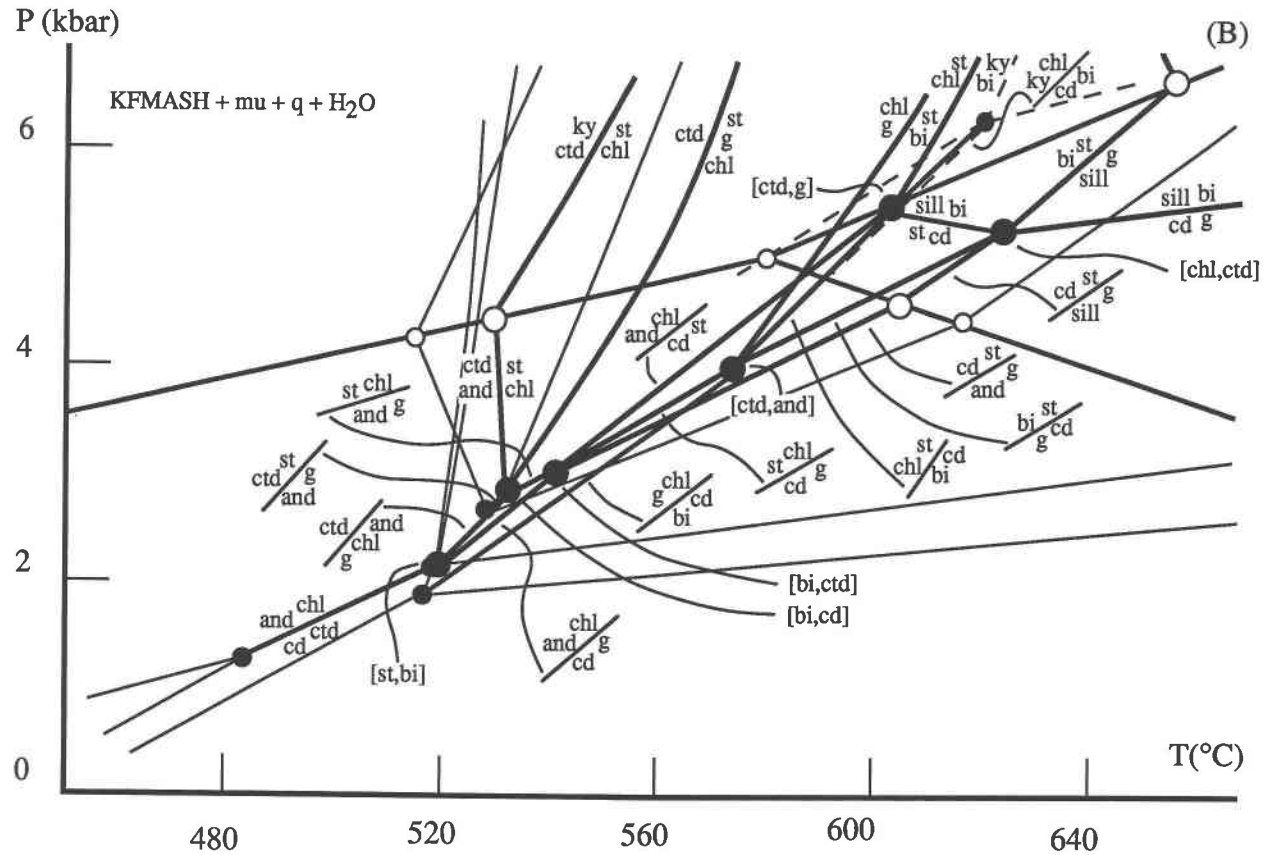

Fig. 2—*Continued.* (**B**) The projection for the andalusite field attempting to label the plethora of reactions occurring there.

counting for petrological observation. Having said that, there are two potential difficulties in the Harte and Hudson approach. First, there are parts of the grid not normally represented in rocks, for example, because rocks would have to be unnaturally Fe rich to "see" the reactions. It is in this situation that we have a considerable advantage over Harte and Hudson because we can calculate the equilibria, whereas they had no petrological constraints to incorporate. Second, given that the Harte and Hudson (1979, Fig. 2) grid is petrologically constrained, it may be difficult to generate a strict KFMASH grid because rocks do not lie in KFMASH; for example it may be difficult to remove the effect of Fe_2O_3, CaO, and MnO. Geologically, this may not be a problem, but it does make comparison with a calculated strict KFMASH grid hazardous. We now compare the grids and show that the correspondence is remarkably good; the differences between them are accounted for by resolving the above potential difficulties in using petrological observations.

In the pressure range 5–9 kbar on Figure 2, we see that the sequence of classic Barrovian isograds and metamorphic zones is correctly predicted, and thus that the positions of the invariant points [g,ctd] and [cd,ctd], and the reactions around them, agree with the grid of Harte and Hudson (1979). Moreover, the temperatures corresponding to these reactions are also in good agreement with the current consensus using conventional thermometry and barometry (see Fig. 7 of Droop, 1985, for staurolite isograd rocks in Austria). However, we predict that garnet is less Fe rich than staurolite, whereas in nature the reverse is found, and the reverse is assumed in the Harte and Hudson grid (e.g., Thompson, 1976). On the grid in Figure 2, mechanically correcting this discrepancy means moving the KFASH reaction st = ky + g to a temperature lower than those reactions with negative dP/dT through [bi,cd] and [ctd,cd] and changing these KFMASH reactions to involve only st on the low temperature side in each case. With this change, the middle reaction must curve to higher temperature relative to the outer two for Schreinemakers's rules to be obeyed.

There may be several reasons for this problem; either our activity model is inappropriate for staurolite or other components in natural staurolites (Fe^{3+}, Zn, Li, etc.; Holdaway et al., 1988) or natural garnets (Ca,Mn) modify the Fe-Mg exchange. Certainly Holdaway et al. (1988) found that garnet/staurolite Fe/Mg partitioning was nonideal and even postulated a large Fe-Mg interaction energy, which

TABLE 1. THERMOCALC results on KFMASH equilbria

	P (kbar)	T (°C)	x_{st}	x_{ctd}	x_{cd}	x_q	x_{chl}	y_{chl}	x_{bi}	y_{bi}	x_{mu}	y_{mu}
(a) Examples of KFMASH univariant reactions												
[ctc,cd,ky]	4.0	578	0.944			0.914	0.617	0.712	0.660	0.497	0.825	0.884
	6.0	608	0.899			0.849	0.480	0.685	0.518	0.461	0.726	0.856
	8.0	633	0.844			0.773	0.374	0.659	0.402	0.426	0.628	0.826
	10.0	653	0.777			0.688	0.289	0.634	0.306	0.393	0.531	0.795
	12.0	670	0.696			0.594	0.219	0.610	0.227	0.361	0.436	0.762
	14.0	685	0.599			0.491	0.160	0.587	0.162	0.332	0.344	0.728
	16.0	699	0.483			0.378	0.110	0.565	0.108	0.304	0.253	0.694
[bi,cd,ky]	4.0	549	0.979	0.943		0.968	0.807	0.721				
	6.0	568	0.959	0.895		0.938	0.691	0.696				
	8.0	583	0.933	0.840		0.902	0.587	0.669				
	10.0	596	0.901	0.778		0.859	0.494	0.643				
	12.0	607	0.862	0.711		0.808	0.411	0.616				
[bi,cd,chl]	10.0	610	0.789	0.591		0.711						
	12.0	607	0.867	0.719		0.815						
	14.0	599	0.954	0.892		0.935						
[bi,cd,g]	4.0	526	0.953	0.878			0.640	0.755				
	6.0	550	0.934	0.837			0.570	0.722				
	8.0	571	0.912	0.796			0.510	0.687				
	10.0	590	0.889	0.754			0.458	0.651				
	12.0	608	0.863	0.712			0.413	0.616				
[bi,cd,ctd]	5.0	643	0.826			0.741	0.337	0.688				
	7.0	641	0.829			0.750	0.348	0.669				
	9.0	632	0.839			0.768	0.367	0.648				
[bi,cd,st]	12.0	607		0.711		0.809	0.412	0.616				
	14.0	613		0.658		0.767	0.356	0.585				
	16.0	618		0.603		0.721	0.307	0.553				
[ctd,cd,chl]	5.0	620	0.916			0.870			0.572	0.496	0.762	0.873
	5.8	640	0.893			0.835			0.513	0.486	0.715	0.863
	6.7	660	0.865			0.796			0.455	0.476	0.666	0.852
	7.6	680	0.833			0.751			0.400	0.465	0.615	0.841
	6.0	659	0.883			0.819			0.495	0.493	0.698	0.863
	7.0	650	0.862			0.793			0.444	0.462	0.659	0.846
	8.0	640	0.841			0.768			0.399	0.431	0.623	0.828
[ctd,cd,g]	5.0	603	0.877				0.419	0.707	0.461	0.498	0.675	0.887
	7.0	624	0.852				0.381	0.676	0.413	0.451	0.636	0.849
	9.0	642	0.826				0.349	0.645	0.372	0.406	0.601	0.806
[ctd,cd,st]	8.0	633				0.771	0.371	0.660	0.399	0.428	0.625	0.828
	10.0	649				0.702	0.301	0.629	0.318	0.384	0.546	0.788
	12.0	663				0.629	0.242	0.598	0.250	0.343	0.470	0.745
	14.0	674				0.551	0.192	0.568	0.193	0.304	0.396	0.699
	16.0	684				0.468	0.148	0.538	0.144	0.269	0.325	0.652
[st,ctd,chl]	5.3	620			0.451	0.859			0.550	0.492	0.746	0.871
	5.4	640			0.453	0.855			0.552	0.493	0.745	0.867
	5.5	660			0.454	0.850			0.554	0.495	0.743	0.862
	5.6	680			0.453	0.845			0.554	0.496	0.741	0.857
[ctd,chl,and]	3.9	560	0.950		0.590	0.924			0.679	0.489	0.840	0.884
	4.3	580	0.939		0.546	0.907			0.639	0.490	0.813	0.880
	4.7	600	0.927		0.504	0.887			0.601	0.491	0.785	0.876
	5.1	620	0.913		0.465	0.866			0.564	0.492	0.756	0.871
[st,ctd,and]	1.9	520			0.930	0.992	0.940	0.722	0.951	0.494	0.980	0.893
	2.6	540			0.798	0.972	0.824	0.717	0.852	0.493	0.934	0.888
	3.4	560			0.673	0.945	0.714	0.713	0.752	0.492	0.881	0.884
	4.2	580			0.560	0.911	0.610	0.708	0.652	0.491	0.821	0.880
(b) Stable KFMASH invariant points												
[bi,cd]	11.9	607	0.864	0.714		0.810	0.414	0.617				
[bi,cd]	2.6	532	0.989	0.970		0.984	0.889	0.738				
[ctd,cd]	8.3	636	0.835			0.761	0.360	0.655	0.386	0.421	0.613	0.822
[ctd,chl]	5.3	627	0.908		0.452	0.858			0.551	0.492	0.746	0.87
[ctd,g]	5.4	608	0.873		0.358		0.414	0.700	0.453	0.487	0.669	0.879
[ctd,bi]	2.8	540	0.983		0.808	0.974	0.834	0.734				
[st,bi]	2.4	527		0.979	0.906	0.989	0.919	0.739				
[ctd,and]	4.4	584	0.936		0.536	0.902	0.589	0.707	0.631	0.491	0.807	0.879
(c) Uncertainties on example univariant equilibria												
g + chl = st + bi (mu, q, H_2O)												
	6.0	608	0.899			0.849	0.480	0.685	0.518	0.461	0.726	0.856
σ		13	0.0241			0.0339	0.0594	0.0107	0.0590	0.0481	0.0489	0.0127
bi + sill = cd + g (mu, q, H_2O)												
	5.7	700			0.452	0.839			0.553	0.497	0.738	0.853
σ	1.0				0.139	0.0739			0.139	0.0603	0.105	0.0138

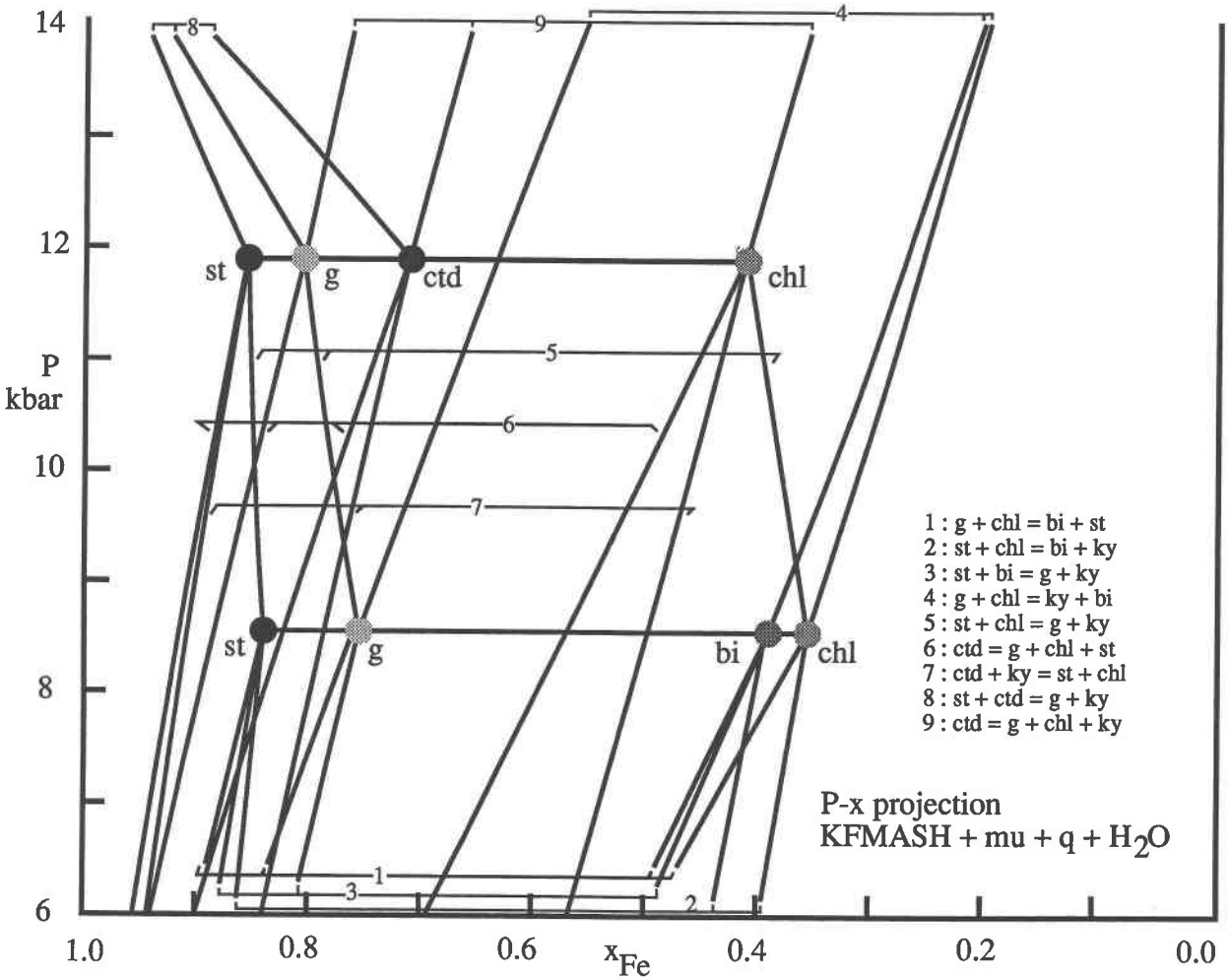

Fig. 3. *P-x* projection for the KFMASH invariant and univariant equilibria in the kyanite field. The diagram summarizes the change of mineral compositions in terms of $MgFe_{-1}$ in univariant mineral assemblages along pressure-temperature reaction lines. As a consequence the diagram must be read in terms of bundles of lines; the key to the labeling in terms of the reactions involved, is provided to the right of the diagram. The bundles will in general involve four lines, but if kyanite is involved in the reaction, three lines are involved.

would result in a miscibility gap closing at 600 °C, to account for their observations. The crystal chemistry of staurolites is still poorly understood, and it is more than likely that Mg does not simply exchange for Fe^{2+} on the four tetrahedral sites as we have assumed. In nature, reversals in K_D are found between staurolite and other minerals (Grambling, 1983; Schreyer et al., 1984; Holdaway et al., 1988) and testify to either severe nonideality in staurolite or to incorrect assumptions as to which sites contain Mg in the more magnesian staurolites. For the wide range of possible substitution schemes the reader is referred to the paper of Holdaway et al. (1987). We cannot add usefully to their discussion, except to note that our Fe/(Fe + Mg) ratios of garnet and staurolite, although the wrong way round, lie within each other's calculated limits of uncertainty. However it is important to emphasize that, apart from this problem, the compositions of the minerals and the way they change along the univariant lines, as well as the calculated temperatures, agree well with what is observed in nature (see the *P-x* projection, Fig. 3).

An additional major problem with our calculated grid is that we do not predict a stability field for biotite + andalusite or for biotite + chloritoid in the simple (Fe^{3+}-absent) KFMASH system, the former assemblage being ubiquitous in low-pressure metamorphic terranes. In a later section we show that both of these assemblages are stable when a small amount of Fe^{3+} is incorporated into biotite and chloritoid.

We have been able to add some information not available to Harte and Hudson when they prepared their grid, which we now discuss. The reaction ctd + g + chl + ky, which leads from the [bi,cd] invariant point at 12 kbar and 600 °C towards higher pressures and temperatures,

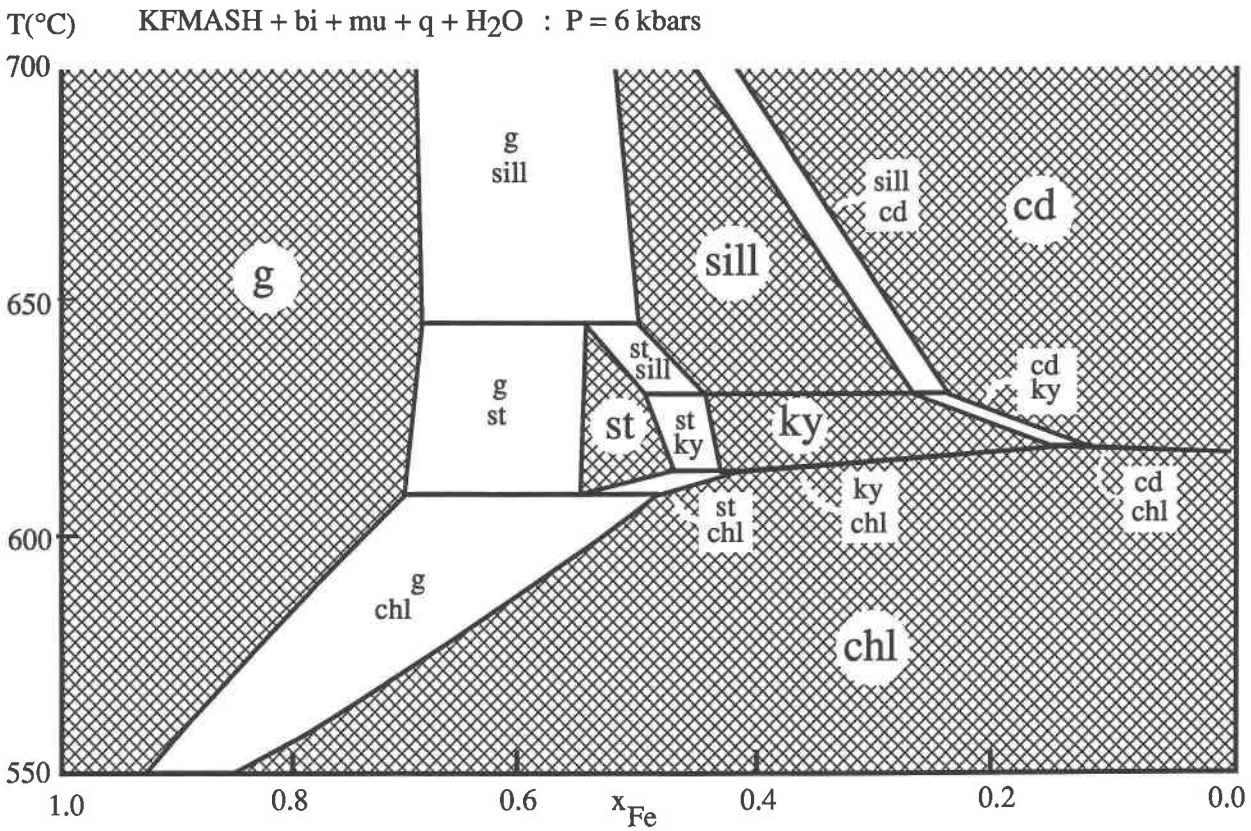

Fig. 4. *T-x* pseudosection for bulk compositions with a range of Fe/(Fe + Mg) at constant Al/(Fe + Mg) below g + chl in AFM; all assemblages involve biotite (see text).

ends in our grid at a MASH invariant point at around 40 kbar and 630 °C, whereas according to Harte and Hudson it ends at an invariant point in FASH (which we calculate to lie at about 2 kbar and 520 °C). At least part of the problem may have come from their assumed compositional degeneracy involving garnet and chlorite. The important consequence for the phase relations is that the compositions of chloritoid, garnet, and chlorite become more magnesian (rather than more Fe rich) as pressures rise along this univariant reaction. Certainly the recent observations of Chopin (1984) and Chopin and Schreyer (1983) in the Western Alps support the extremely magnesian compositions attainable in this assemblage at high pressure.

The Harte and Hudson grid does not allow the mutual compatibility of cordierite + garnet; the incompatibility comes about because of two features built into their grid, namely, (1) their reaction st + cd = a + bi has large dP/dT and (2) their reaction st = bi + a + g has a negative slope. This geometry, which excludes their intersection to generate the reaction bi + a = cd + g, was deliberately implemented by Harte and Hudson on the basis of experimental observations of Holdaway and Lee (1977). In our grid, it is the flat negative slope of st + cd = sill + bi coupled with the flat positive slope of st + bi = a + g in the sillimanite field that allows their intersection [chl,ctd] at around 4.5 kbar and 620 °C. The sharp change in slope of the st + bi = a + g reaction at the ky = sill boundary is remarkable and would have been hard to foresee when Harte and Hudson created their grid. In fact, in our grid there are reactions involving g + cd with decreasing temperature and pressure until and + chl = g + cd terminates in a KFASH invariant point at about 520 °C and 2 kbar (Fig. 2b). However, at temperatures lower than 575 °C, g + cd can only occur in compositions more aluminous than g + chl, and only in Fe-rich compositions.

The difference between our grid and that of Harte and Hudson in the andalusite field is due partly to the g + cd equilibria problem discussed above, but it is mainly due to the difficulty that few if any rocks "see" anything other than equilibria involving some of bi, chl, cd and and, with assemblages changing via KFMASH divariant or trivariant equilibria. They chose to represent the low-pressure region in the simplest way possible: we were certainly surprised to see the mess of reactions we calculated at low pressure! Lobotka (1981, Fig. 11) also deduced a complex net of equilibria at low pressures; he also indicated stability of garnet + cordierite at the low pressure end of his grid.

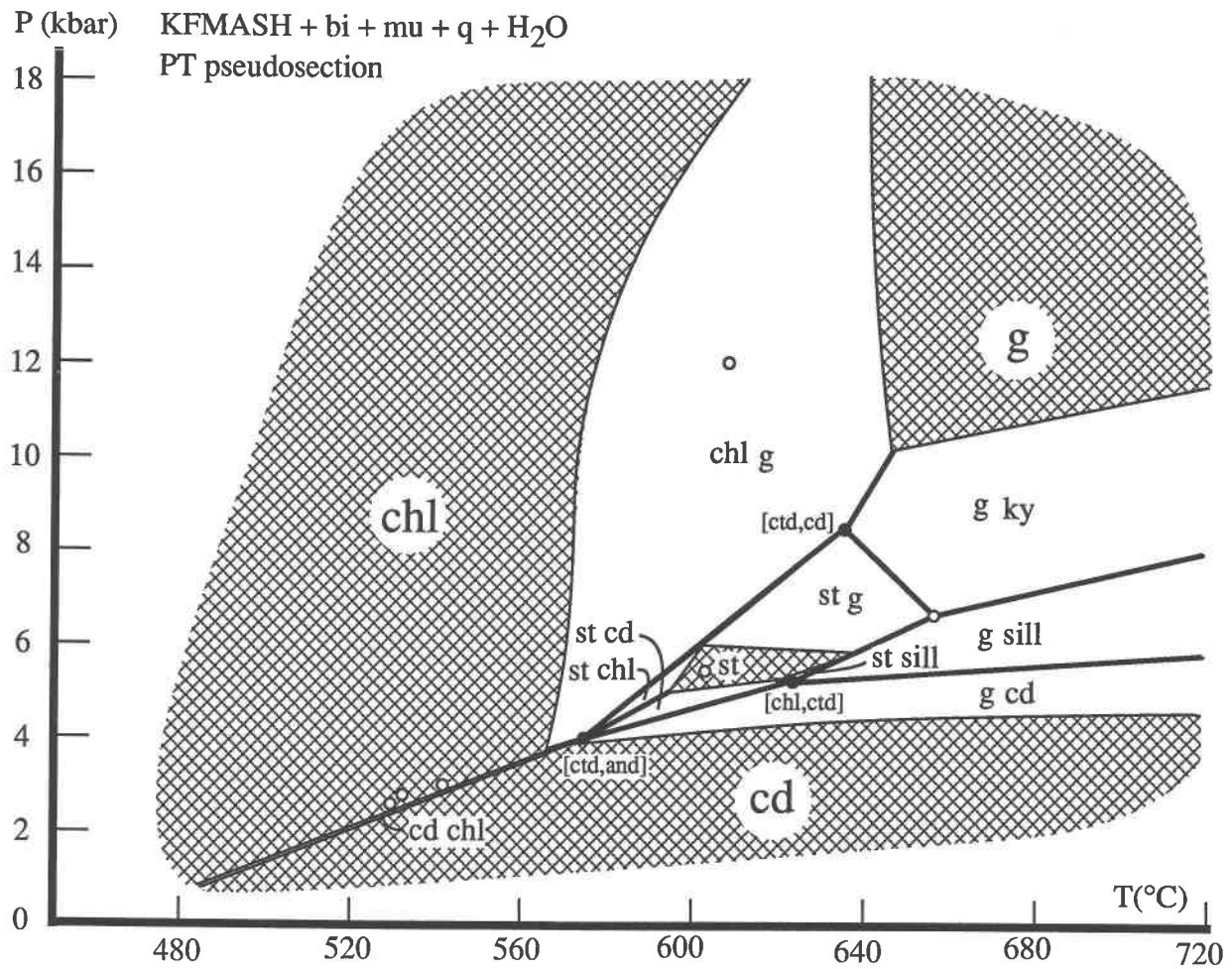

Fig. 5. *P-T* pseudosection for a bulk composition with Fe/(Fe + Mg) = 0.7 and a Al/(Fe + Mg) below g + chl in AFM; all assemblages involve biotite. The black dots are KFMASH invariant points included for reference. Note (1) the shape of the g + chl divariant field is controlled by the curvature of the KFASH univariant reactions; (2) the simplicity of the fields at lower pressure compared with the complexity of Fig. 2b; and (3) the nature of the single phase staurolite field.

KFMASH + Fe_2O_3

In the absence of thermodynamic data for ferri-annite, for example, it is not yet possible to calculate equilibria in the KFMASHO system. However, it is possible to perform semiquantitative calculations by recalculating the equilibria of interest for fixed proportions of Fe^{3+} incorporated in the minerals. The resulting diagrams will not be correct because the incorporation of Fe^{3+} in the minerals will change along the univariant lines. However, such calculations do indicate the sense in which the equilibria will change in going from KFMASH into KFMASHO. In terms of this system we assume that biotite and chloritoid are the main minerals stabilized by the incorporation of Fe^{3+}.

Figure 6 shows the effect of incorporating increasing Fe^{3+} into biotite, with n% referring to the proportion of Fe^{3+} added in terms of $Fe^{3+}/(Fe^{3+} + Al^{oct})$. With only 10% added, a substantial andalusite + biotite field is created as the [ctd,g] and [chl,cd] invariant points are displaced to lower *P-T* along the [bi] reactions emanating out of these invariant points. By 10% addition the equilibria have collapsed on the stationary [bi,ctd]. The effect of concomitant addition of Fe^{3+} into chloritoid is not included on this diagram, although clearly the position of the [bi,ctd] invariant point will be largely unaffected by addition of Fe^{3+}. Thus, with consideration of Fe^{3+}, a large biotite + andalusite field is generated; the field is even larger if the uncertainty on the the position of sill + bi = g + cd is also taken into account. The main difference between Figure 6 and Figure 2 is that the rather unusual assemblage staurolite + cordierite, which had a rather large field in the KFMASH grid, disappears. If our logic is correct, staurolite + cordierite may be seen in nature only rarely because it requires rather reducing conditions. Further, the stability of g + cd is substantially reduced.

Figure 7 shows the effect of incorporating 15% Fe^{3+} in

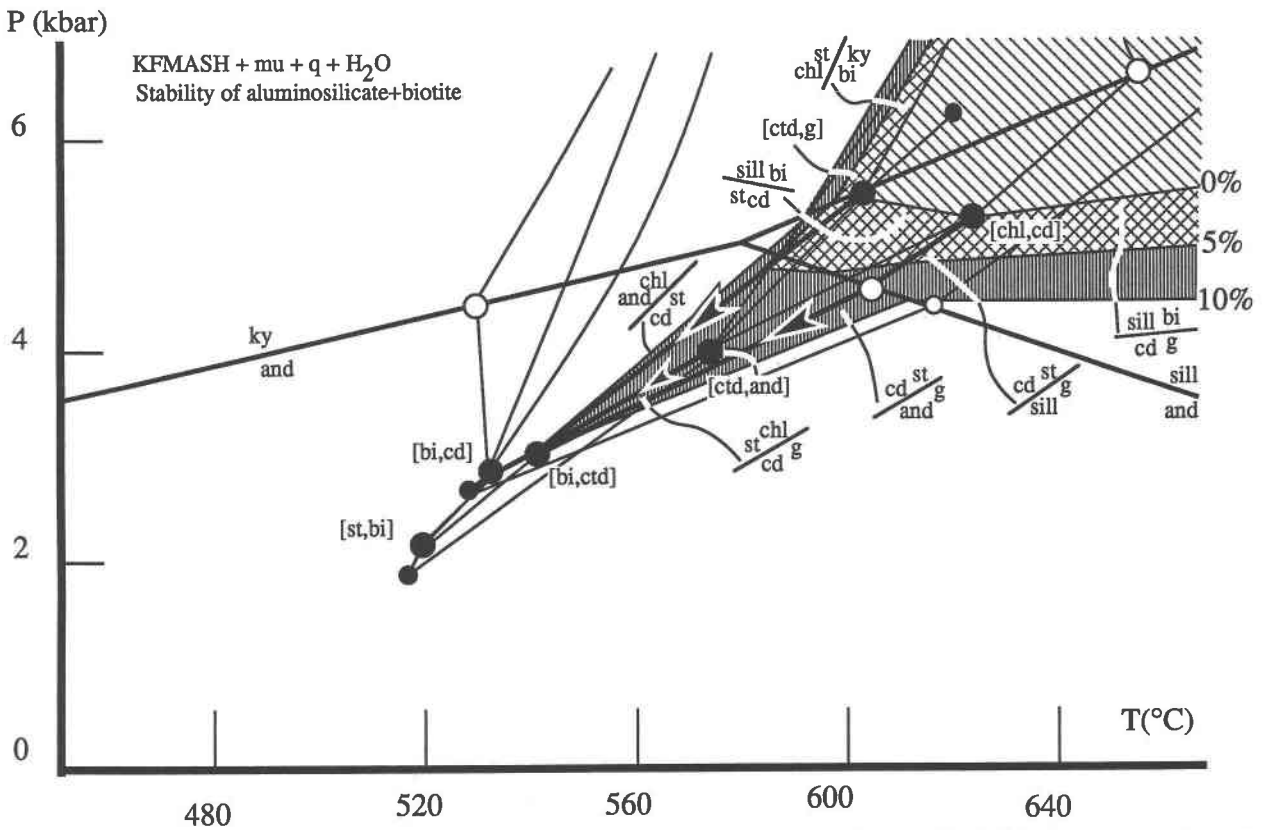

Fig. 6. The effect of adding Fe^{3+} to biotite on the stability of aluminosilicate + biotite. The label of 10% on the boundary of the shaded region indicates substitution of 10% of octahedral Al by Fe^{3+}. On addition of Fe^{3+} to biotite, the [ctd,g] and [chl,cd] invariant points move down the bold lines indicated by arrows, which are [bi] reactions. With reference to Fig. 2b, the expansion of the andalusite + biotite field primarily occludes the staurolite + chlorite field.

octahedral sites in biotite and 10% Fe^{3+} in octahedral sites in chloritoid, with [cd,bi] approaching [cd,ctd] along their connecting reaction, allowing the creation of [cd,ky] when ctd = chl + g + st intersects chl + g = bi + st. With this invariant point stable, a chloritoid + biotite stability field expands to lower pressures. The size of this field is dependent on the amount of Fe^{3+} incorporated in the phases; it is certainly possible for reduced assemblages not to have access to this field, or for bi-ctd- and g-chl-bearing assemblages to be interlayered in rocks, if for example different Fe-Ti oxide assemblages are present.

As a consequence of the consideration of the incorporation of Fe^{3+} in the minerals, the correspondence between our grid and that of Harte and Hudson, and thus the correspondence with petrological observation, is much better. The work of Guidotti (1974) and of Holdaway et al. (1982) on pelites in Maine shows that a transition from the staurolite to the sillimanite zone may occur via the reaction st + chl + mu = bi + sill + H_2O. In our pure KFMASH grid this reaction can occur only in the kyanite field (Fig. 2) but would become possible with the addition of some Fe^{3+} and a lower-temperature aluminosilicate triple point (Figs. 6, 7). In using our grids the reader must allow considerable flexibility in the position of the and = sill boundary, as in nature it will certainly vary from one set of rocks to another (see discussion section and Salje, 1986). The major remaining difference between our grid and that of Harte and Hudson is in the stability of garnet + cordierite with muscovite + quartz. We might add that qualitatively extending our grid into the granulite facies with quartz, alkali feldspar and melt in excess is made easier by the stability of bi + sill = g + cd, it being deflected to steeper slopes across the mu + q breakdown reaction and across the solidus, to become the classic lowermost granulite facies reaction.

Discussion

The KFMASH grid presented here, calculated from the internally consistent data set of Holland and Powell (1990), appears to correspond well to petrological observation, apart from the difficulties with the low pressure equilibria discussed above. This correspondence must relate to the quality of the experimental data on mineral equilibria used in the thermodynamic data extraction and be a testament to the activity-composition models used. We do not pretend that the grid in Figure 2 is the last word in KFMASH; as outlined in Holland and Powell

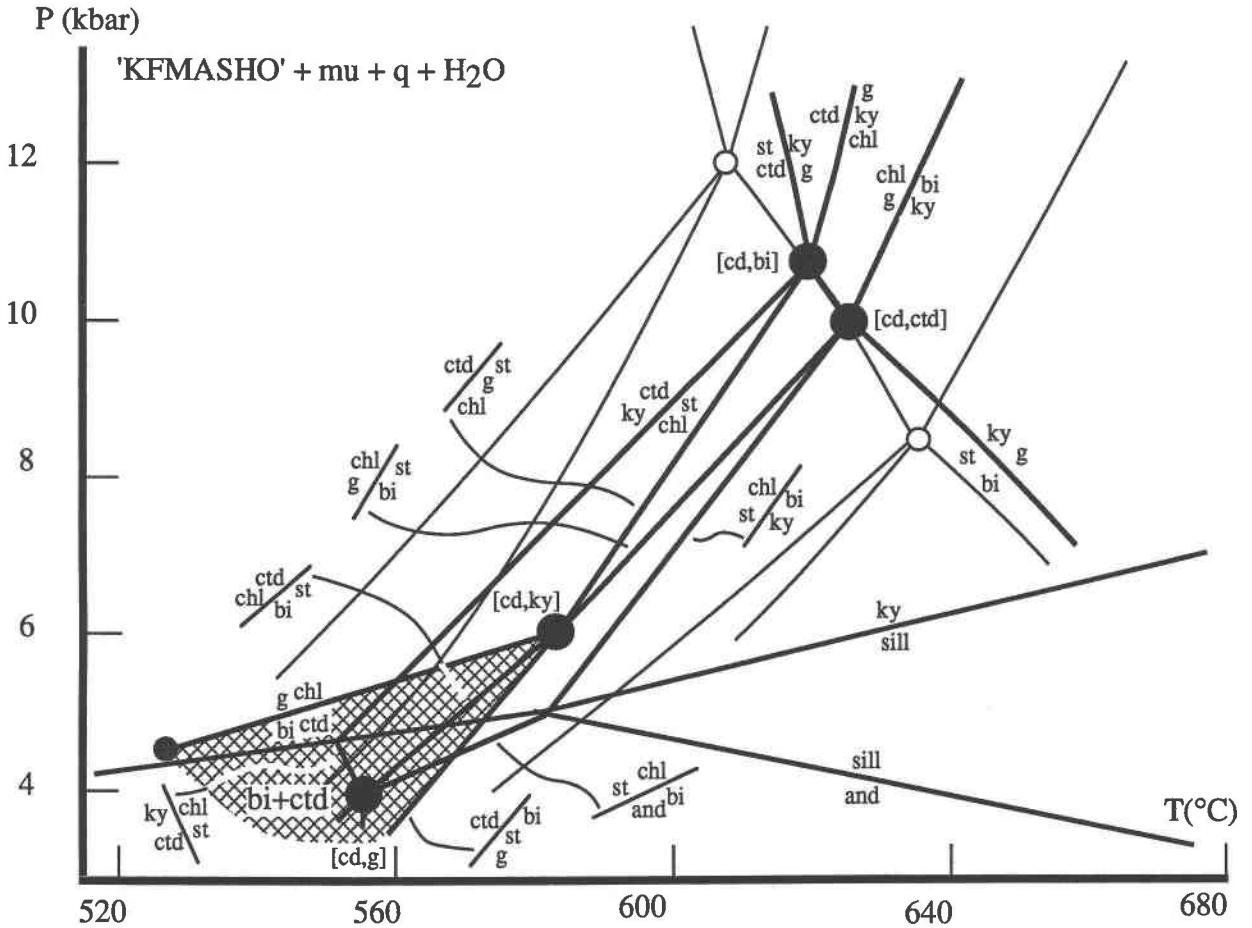

Fig. 7. The effect of adding Fe^{3+} to octahedral sites in biotite (15%) and chloritoid (10%) on the stability of the assemblage chloritoid + biotite. The stabilizing of biotite and chloritoid closes the pressure gap between [cd,bi] and [cd,ctd], creating [cd,ky], and stabilizing a chloritoid + biotite field to lower pressure (shaded). Note that, with reference to Fig. 2a, this field is not stable in the strict KFMASH grid. The *P-T* location of [cd,ky] is in good agreement with that deduced from thermobarometry by Droop (1981, 1985).

(1990) the experimentally determined FASH equilibria are not handled completely satisfactorily, and the Tschermak-substituted end-members (east, ames, cel, fcel) are not yet well constrained. The former of these problems may be caused by the poor characterization of staurolite and/or experimental difficulties; the latter by the paucity of appropriate experimental constraints.

The predictions of the Tschermak's substitutions in minerals as a function of grade and assemblage are in reasonable agreement with natural data. We mentioned the chlorite compositions earlier as being in agreement with the data compiled by Laird (1988), and these trends are fairly general: chlorites, biotites, and phengites tend to become more aluminous with increasing temperature and with decreasing pressure. This trend in phengites is now well established (e.g., Guidotti, 1973, 1984; Chopin, 1984). Our calculated alumina contents in biotite vary from close to the phlogopite-annite join ($y_{bi} = 0$) at high pressures and low temperatures to halfway between that and the eastonite-siderophyllite join ($y_{bi} = 1$) at high temperatures and low pressures. The values calculated are rarely above $y_{bi} = 0.5$, in excellent agreement with Guidotti (1984, Fig. 35, p. 420), who showed that natural biotites appear to be restricted to y_{bi} in the region of 0 to a little over 0.5. Obviously the simple trends noted above will be modified by the fact that the maximum aluminum content also depends on the coexisting assemblage.

Although the paucity of data on Tschermak's substituted end-members in minerals is a problem, our results indicate that this aspect of the solid solutions should not be ignored, because the $(Fe,Mg)SiAl_{-2}$ of the minerals may change dramatically along reaction lines, thus affecting their slope. However, Spear and Cheney (1989) assumed that the solid solutions involve the substitution $FeMg_{-1}$ but not $(Fe,Mg)SiAl_{-2}$, and some features of their grid seem to be a consequence of that: for example, the absence of low pressure KFASH and KFMASH invariant points. Further, by analogy with our calculations, their

KFASH reactions chl = ctd + bi and ctd + bi = g would converge to higher pressure if (Fe,Mg)$SiAl_{-2}$ in chlorite, particularly, were allowed to change along the reaction lines. That their reactions converge to lower pressure leads to the "wrong-way-around" reaction ctd + bi = g + chl, and thus to an unusual topology of ctd-bearing reactions at higher pressures. They propose the addition of Mn to "reverse" the reaction; although possible, this would require rather nonideal mixing of Mn, Fe, and Mg.

The appearance of bi + and and the absence of g + cd in (mu + q)–bearing assemblages in rocks in low pressure terranes may not be entirely satisfactorily explained by consideration of the addition of Fe_2O_3 to KFMASH, even when uncertainties in the calculated equilibria are considered. This problem might be resolved, for example, if biotite, via its eastonite end-member, were somewhat more stable; this solution would not only increase the stability field of bi + and, but also of bi + st and bi + cd. It is interesting that Spear and Cheney also appeared to have a difficulty with the "excess" stability of g + cd (Spear and Cheney, 1989, p. 154). The careful work of Droop (1981, 1985) on pelites from the Tauern window of Austria is nicely explained by our grid when some Fe^{3+} is added to the KFMASH system: Droop (1985) indicates, on the basis of a number of thermometers and barometers, that the g + chl + mu = st + bi isograd occurs at about 7 kbar and 580 °C in this kyanite-bearing terrane, in reasonable agreement with our Figure 7. Droop's earlier work (1981, Figs. 12, 13) shows that his slightly lower pressure rocks developed assemblages with chloritoid + biotite; thus his two suites record conditions of pressure just above and just below the invariant point [cd,ky], which occurs at about 6 kbar and 580 °C on our Figure 7.

To those who prefer a lower temperature aluminosilicate triple point, it is important to realize that the form of the grid in Figure 2 is little affected by moving the triple point along the major principal axis of the uncertainty ellipse on this point (Powell and Holland, 1988); the axis corresponds to the overlap on the (narrow) uncertainties on the positions of ky = and and ky = sill. Moving the triple point mainly moves and = sill; as the thermodynamic properties (ΔV, ΔS, ΔG) of this reaction are very small, most reactions are little inflected in crossing it. The petrological arguments concerning the position of the triple point in natural terranes seem to be conflicting, and this is not the place for a proper discussion. On the one hand, a lower temperature is implied by ctd + sill, but a higher one for st + and. On the basis of our grid, we would consider a lower temperature limit of 540 °C for the triple point; this is in fact within our calculated uncertainty on the position of the triple point. Of course, the position of the and = sill reaction in any set of natural rocks may be quite variable and will depend chiefly upon the defect density in the sillimanite concerned (Salje, 1986). It is only in the probably rare situation of defect-free sillimanite that a lower temperature triple point is appropriate.

We believe that the use of an internally consistent data set is the best way to generate petrogenetic grids. Such data sets can involve a combination of all available experimental data. Moreover, reliable petrological data can be incorporated with all the other data; we have incorporated some data on element exchanges into our data set (Holland and Powell, 1990). We are concerned that the approach of Spear and Cheney, in incorporating only a minimum amount of data, experimental or petrological, is going to be critically dependent on the data chosen and the assumptions made. However it is done, it is important that all the reliable data, experimental and petrological, are combined. Currently we have incorporated limited petrological data, partly recognizing the difficulty of constraining the conditions of formation of rocks, partly out of a wish to remain as independent as possible from petrological prejudice (and thus avoiding circularity of arguments), and partly recognizing the difficulty of constraining subsystem equilibria in rocks.

As the conditions of formation of rocks and activity-composition relations in minerals become better known, more rock data will be incorporated in our data set. As new experimental data become available, the thermodynamic data can be better constrained; further progress will be difficult without new experimental work, particularly to improve the thermodynamic data for Fe-bearing cordierites and staurolites. Moreover, as argued above, rocks rarely lie in KFMASH, with at least Fe_2O_3 being important, if not CaO, Na_2O, and MnO. Until Fe_2O_3 can be properly incorporated, it will be difficult to know if the above logic is appropriate. The grid will certainly be more realistic when CaO and Na_2O can be incorporated and plagioclase included; this step awaits the development of appropriate activity-composition models for garnet and plagioclase.

Acknowledgments

We would like to thank Graham Chinner, Ben Harte, Jo Laird, and an intemperate anonymous reviewer for comments; we hope the paper is much improved as a consequence of their help. Cambridge Earth Sciences contribution ES 1403.

References cited

Albee, A.L. (1965) A petrogenetic grid for the Fe-Mg silicates of pelitic schists. American Journal of Science, 263, 512–536.

Chopin, C. (1984) Coesite and pure pyrope in high-grade blueschists of the Western Alps; a first record and some consequences. Contributions to Mineralogy and Petrology, 86, 107–118.

Chopin, C., and Schreyer, W. (1983) Magnesio-carpholite and magnesio-chloritoid: Two index minerals of pelitic blueschists and their preliminary phase relations in the model system MgO-Al_2O_3-SiO_2-H_2O. American Journal of Science, 283A, 72–96.

Droop, G.T.R. (1981) Alpine metamorphism of peliteic schists in the south-east Tauern Window, Austria. Schweizerische Mineralogische und Petrographische Mitteilungen, 61, 237–273.

——(1985) Alpine metamorphism in the south-east Tauern Window, Austria: 1. *P-T* variations in space and time. Journal of Metamorphic Geology, 3, 371–402.

Grambling, J.A. (1983) Reversals in Fe-Mg partitioning between chloritoid and staurolite. American Mineralogist, 68, 373–388.

Guidotti, C.V. (1973) Compositional variation of muscovite as a function

of metamorphic grade and assemblage in metapelites from northwestern Maine. Contributions to Mineralogy and Petrology, 42, 33–42.

——— (1974) Transition from the staurolite to sillimanite zone, Rangely Quadrangle, Maine. Geological Society of America Bulletin, 85, 475–490.

——— (1984) Micas in metamorphic rocks. In Mineralogical Society of America Reviews in Mineralogy, 13, 357–468.

Guiraud, M., Holland, T.J.B., and Powell, R. (1989) Mineral equilibria at glaucophane schist to eclogite facies in the system Na_2O-MgO-FeO-Al_2O_3-SiO_2-H_2O. Contributions to Mineralogy and Petrology, in press.

Harte, B. (1975) Determination of a pelite petrogenetic grid for the eastern Scottish Dalradian. Yearbook of the Carnegie Institution of Washington, 74, 438–446.

Harte, B., and Hudson, N.F.C. (1979) Pelite facies series and the temperatures and pressures of Dalradian metamorphism in eastern Scotland. In The Caledonides of the British Isles Reviewed, Geological Society of London, Special Publication, 8, 323–337.

Hensen, B.J. (1971) Theoretical phase relations involving cordierite and garnet in the system FeO-MgO-Al_2O_3-SiO_2. Contributions to Mineralogy and Petrology, 31, 191–214.

Hess, P.C. (1969) The metamorphic paragenesis of cordierite in pelitic rocks. Contributions to Mineralogy and Petrology, 24, 191–207.

Holdaway, M.J., and Lee, S.M. (1977) Fe-Mg cordierite stability in high grade pelitic rocks based on experimental and natural observations. Contributions to Mineralogy and Petrology, 63, 175–198.

Holdaway, M.J., Dutrow, B.L., and Hinton, R.W. (1988) Devonian and Carboniferous metamorphism in west-central Maine: The muscovite-almandine geobarometer and the staurolite problem revisited. American Mineralogist, 73, 20–47.

Holdaway, M.J., Dutrow, B.L., Borethwick, J., Shore, P., Harmon, R.S., and Hinton, R.W. (1987) H content of staurolite as determined by H extraction line and ion microprobe. American Mineralogist, 71, 1135–1142.

Holdaway, M.J., Guidotti, C.V., Novak, J.M., and Henry, W.E. (1982) Polymetamorphism in medium- to high-grade pelitic metamorphic rocks, west-central Maine. Geological Society of America Bulletin, 93, 572–584.

Holland, T.J.B., and Powell, R. (1985) An internally consistent thermodynamic dataset with uncertainties and correlations: 2. Data and results. Journal of Metamorphic Geology, 3, 343–370.

Holland, T.J.B., and Powell, R. (1990) An enlarged and updated internally consistent thermodynamic dataset with uncertainties and correlations: The system K_2O-Na_2O-CaO-MgO-MnO-FeO-Fe_2O_3-Al_2O_3-TiO_2-SiO_2-C-H_2-O_2. Journal of Metamorphic Geology, 8, 89–124.

Kurepin, V.A. (1985) H_2O and CO_2 contents of cordierite as an indicator of thermodynamic conditions of formation. Geochemistry International, 22, no. 1, 148–156.

Labotka, T.C. (1981) Petrology of an andalusite-type region metamorphic terrain, Panamint Mountains, California. Journal of Petrology, 22, 261–296.

Laird, J. (1988) Chlorites: Metamorphic petrology. In Mineralogical Society of America Reviews in Mineralogy, 19, 405–453.

Powell, R. (1978) Equilibrium thermodynamics in petrology, 295 p. Harper and Row, London.

——— (1988) An internally consistent thermodynamic dataset with uncertainties and correlations: 3. Applications to geobarometry, worked examples and a computer program. Journal of Metamorphic Geology, 6, 173–204.

Salje, E. (1986) Heat capacites and entropies of andalusite and sillimanite: The influence of fibrolitization on the phase diagram of the Al_2SiO_5 polymorphs. American Mineralogist, 71, 1366–1371.

Schreyer, W., Horrocks, P.C., and Abraham, K. (1984) High-magnesium staurolite in a sapphirine-garnet rock from the Limpopo belt, southern Africa. Contributions to Mineralogy and Petrology, 86, 200–207.

Spear, F.S., and Cheney, J.T. (1989) A petrogenetic grid for pelitic schists in the system SiO_2-Al_2O_3-FeO-MgO-K_2O-H_2O. Contributions to Mineralogy and Petrology, 101, 149–164.

Thompson, A.B. (1976) Mineral reactions in pelitic rocks: II. Calculation of some *P-T-X*(Fe-Mg) phase relations. American Journal of Science, 276, 425–454.

Thompson, A.B., Lyttle, P.T., and Thompson, J.B., Jr. (1977) Mineral reactions and A-Na-K and A-F-M facies types in the Gassetts Schist, Vermont. American Journal of Science, 277, 1124–1151.

Thompson, J.B., Jr. (1957) The graphical analysis of mineral assemblages in pelitic schists. American Mineralogist, 42, 842–858.

——— (1979) The Tschermak substitution and reactions in pelitic schists. In V.A. Zharikov, V.I. Fonarev, and S.P. Korikovskii, Eds., Problems in physicochemical petrology (in Russian) p. 146–159. Academy of Sciences, Moscow.

Will, T., Powell, R., Holland, T.J.B., and Guiraud, M. (1990) Mineral equilibria at greenschist facies conditions in the system CaO-MgO-FeO-Al_2O_3-SiO_2-H_2O-CO_2. Contributions to Mineralogy and Petrology, in press.

Manuscript received February 16, 1989
Manuscript accepted November 9, 1989

Appendix 1. Mineral formulae, end-members, and compositional variables

In the mineral formulae discussed here, $(i,j)_n$ means that i and j substitute for each other on a site, of which there are n in the formula; in these end-member formulae, $(i_n j_m)$ means that n i atoms and m j atoms share a site, of which there are $(n + m)$ in the formula. In the absence of brackets, a particular element completely fills the corresponding site. The activities a_i were formulated using ideal mixing on sites (e.g., Powell, 1978); the specification of sites is discussed in Holland and Powell (1990). □ denotes a site vacancy.

● chloritoid (ctd) $(Fe,Mg)Al_2SiO_5(OH)_2$

variable: $x_{ctd} = Fe/(Fe + Mg)$

end-members: Mg-chloritoid (mctd) $MgAl_2SiO_5(OH)_2$

$a_{mctd} = 1 - x_{ctd}$

Fe-chloritoid (fctd) $FeAl_2SiO_5(OH)_2$

$a_{fctd} = x_{ctd}$

● garnet (g) $(Fe,Mg)_3Al_2Si_3O_{12}$
variable: $x_g = Fe/(Fe + Mg)$
end-members: pyrope (py) $Mg_3Al_2Si_3O_{12}$
$a_{py} = (1 - x_g)^3$
almandine (alm) $Fe_3Al_2Si_3O_{12}$
$a_{alm} = x_g^3$

● chlorite (chl) $(Fe,Mg)_4(Fe,Mg,Al)_2Si_2(Si,Al)_2O_{10}(OH)_8$
variables: $x_{chl} = Fe/(Fe + Mg)$
$y_{chl} = x_{AlM2}$
end-members: clinochlore (clin) $Mg_4(Mg_1Al_1)Si_2(Si_1Al_1)O_{10}(OH)_8$ $(y_{chl} = 0.5)$
$a_{clin} = 16(1 - x_{chl})^5(1 - y_{chl})^2y_{chl}^2$
daphnite (daph) $Fe_4(Fe_1Al_1)Si_2(Si_1Al_1)O_{10}(OH)_8$ $(y_{chl} = 0.5)$
$a_{daph} = 16x_{chl}^5(1 - y_{chl})^2y_{chl}^2$
amesite (ames) $Mg_4Al_2Si_2Al_2O_{10}(OH)_8$ $(y_{chl} = 1)$
$a_{ames} = (1 - x_{chl})^4y_{chl}^4$

● muscovite (mu) $K\square(Al,Mg,Fe)_2Si_2(Al,Si)_2O_{10}(OH)_2$
variable: $x_{mu} = Fe/(Fe + Mg)$
$y_{mu} = 2x_{AlT2}$
end-members: muscovite (mu) $K\square(Al_2Si_2(Al_1Si_1)O_{10}(OH)_2$ $(y_{mu} = 1)$
$a_{mu} = 0.25(1 + y_{mu})^2(2 - y_{mu})y_{mu}$
celadonite (cel) $K\square(Al_1Mg_1)Si_2(Si_2)O_{10}(OH)_2$ $(y_{mu} = 0)$
$a_{cel} = 0.25(1 - x_{mu})(2 - y_{mu})^2(1 + y_{mu})(1 - y_{mu})$
ferroceladonite (fcel) $K\square(Al_1Fe_1)Si_2(Si_2)O_{10}(OH)_2$ $(y_{mu} = 0)$
$a_{fcel} = 0.25x_{mu}(2 - y_{mu})^2(1 + y_{mu})(1 - y_{mu})$

● biotite (bi) $K(Mg,Fe)(Al,Mg,Fe)_2Si_2(Al,Si)_2O_{10}(OH)_2$
variable: $x_{bi} = Fe/(Fe + Mg)$
$y_{bi} = 2x_{AlM2}$
end-members: phlogopite (phl) $KMgMg_2Si_2(Al_1Si_1)O_{10}(OH)_2$ $(y_{bi} = 0)$
$a_{phl} = 0.25(1 - x_{bi})^3(2 - y_{bi})^2(1 + y_{bi})(1 - y_{bi})$
annite (ann) $KFeFe_2Si_2(Al_1Si_1)O_{10}(OH)_2$ $(y_{bi} = 0)$
$a_{ann} = 0.25x_{bi}^3(2 - y_{bi})^2(1 + y_{bi})(1 - y_{bi})$
eastonite (east) $KMg(Mg_1Al_1)Si_2(Al_2)O_{10}(OH)_2$ $(y_{bi} = 1)$
$a_{east} = 0.25(1 - x_{bi})^2y_{bi}(1 + y_{bi})^2(2 - y_{bi})$

● cordierite (cd) $(Mg,Fe)_2Al_4Si_5O_{18}$
variables: $x_{cd} = Fe/(Fe + Mg)$
end-members: cordierite (crd) $Mg_2Al_4Si_5O_{18}$
$a_{crd} = (1 - x_{cd})^2$
iron cordierite (fcrd) $Fe_2Al_4Si_5O_{18}$
$a_{fcrd} = x_{cd}^2$
(H_2O incorporated via Kurepin's (1985) model)

● staurolite (st) $(Mg,Fe)_4Al_{18}Si_{7.5}O_{48}H_4$
variable: $x_{st} = Fe/(Fe + Mg)$
end-members: staurolite (st) $Fe_4Al_{18}Si_{7.5}O_{48}H_4$
$a_{st} = x_{st}^4$
magnesiostaurolite (mst) $Mg_4Al_{18}Si_{7.5}O_{48}H_4$
$a_{mst} = (1 - x_{st})^4$

● kyanite (ky) Al_2SiO_5 $a_{ky} = 1$

● quartz (q) SiO_2 $a_q = 1$

● H_2O (H_2O) H_2O $a_{H_2O} = 1$